Inorg. Chem. **2008**, *47*, 8204−8212

Synthesis, Structure, and High-Temperature Thermoelectric Properties of Boron-Doped $Ba_8Al_{14}Si_{31}$ Clathrate I Phases

Cathie L. Condron,[†,⊥] Susan M. Kauzlarich,[*,†] Teruyuki Ikeda,[‡,§] G. Jeffrey Snyder,[‡,§] Frank Haarmann,[||] and Peter Jeglič[||,#]

Department of Chemistry, University of California, One Shields Ave., Davis, California 95616, Jet Propulsion Laboratory, California Institute of Technology, 4800 Oak Grove Drive, Pasadena, California 91109-8099, Materials Science, California Institute of Technology, 1200 California Blvd., Pasadena, California 91125, and Max-Planck-Institut für Chemische Physik fester Stoffe, Nöthnitzer Str. 40, 01187 Dresden, Germany

Received April 29, 2008

Single crystals of boron-doped $Ba_8Al_{14}Si_{31}$ clathrate I phase were prepared using Al flux growth. The structure and elemental composition of the samples were characterized by single-crystal and powder X-ray diffraction; elemental analysis; and multinuclear ^{27}Al, ^{11}B, and ^{29}Si solid-state NMR. The samples' compositions of $Ba_8B_{0.17}Al_{14}Si_{31}$, $Ba_8B_{0.19}Al_{15}Si_{31}$, and $Ba_8B_{0.32}Al_{14}Si_{31}$ were consistent with the framework-deficient clathrate I structure $Ba_8Al_xSi_{42-3/4x}\square_{4-1/4x}$ ($x = 14$, $\square$ = lattice defect). Solid-state NMR provides further evidence for boron doped into the framework structure. Temperature-dependent resistivity indicates metallic behavior, and the negative Seebeck coefficient indicates that transport processes are dominated by electrons. Thermal conductivity is low, but not significantly lower than that observed in the undoped $Ba_8Al_{14}Si_{31}$ prepared in the same manner.

Introduction

A good thermoelectric material should have three main properties: a large Seebeck coefficient (S), a low electrical resistivity (ρ) corresponding to high electrical conductivity (σ), and a low thermal conductivity (κ). Together, these three properties act to increase the dimensionless figure of merit ($zT = S^2\sigma/\kappa T$), which is an indicator of a thermoelectric material's efficiency. Typically, a material is thought to require specific characteristics in order to maximize zT, including a large unit cell volume (>1000 Å^3), structural complexity, heavy main group elements, and a small band gap. However, a large unit cell along with heavy elements results in a heavy (high-density) material and is disadvantageous for transportation applications. Additionally, many heavy elements used in thermoelectric materials, such as Pb, As, and Sb, are toxic and environmentally unfriendly. Therefore, in the hopes of creating light element materials that are advantageous for transportation applications, as well as environmentally friendly materials, clathrate phases containing Al/Si frameworks were chosen as a starting point.

Clathrate phases contain some of the typical characteristics typically thought to fulfill the properties needed to achieve a large zT, namely, clathrates possess a large unit cell and structural complexity. In addition, clathrates are stable over a large temperature range. Furthermore, clathrates are stable in the air, moisture, and dilute acids and have inherently low lattice thermal conductivity, and most importantly the clathrate structure allows for controlled manipulation of electronic and thermal transport properties.

Thus far, we have presented the synthesis, crystal structure, Raman spectroscopy, and magnetism of Ba/Eu Al−Si-containing clathrate phases,[1] as well as the single-crystal neutron diffraction, magic angle spinning nuclear magnetic resonance (MAS NMR), and thermoelectric properties of $Ba_8Al_{14}Si_{31}$.[2] These compounds, prepared via Al flux synthesis, are all framework-deficient and can be described via

* Author to whom correspondence should be addressed. E-mail: smkauzlarich@ucdavis.edu.
† University of California.
‡ Jet Propulsion Laboratory, California Institute of Technology.
§ Materials Science, California Institute of Technology.
|| Max-Planck-Institut für Chemische Physik fester Stoffe.
⊥ Current address: Stanford Synchrotron Radiation Laboratory, 2575 Sand Hill Road, Menlo Park, CA 94025.
Current address: Jožef Stefan Institute, Jamova 39, Ljubljana 1000, Slovenia.

(1) Condron, C. L.; Porter, R.; Guo, T.; Kauzlarich, S. M. *Inorg. Chem.* **2005**, *44*, 9185.
(2) Condron, C. L.; Martin, J.; Nolas, G. S.; Piccoli, P. M. B.; Schultz, A. J.; Kauzlarich, S. M. *Inorg. Chem.* **2006**, *45*, 9381.

10.1021/ic800772m CCC: $40.75
Published on Web 08/19/2008

the formula $Ba_8Al_xSi_{42-3/4\ x}\square_{4-1/4\ x}$ ($x = 14$, $\square$ = lattice defect). The single-crystal neutron refinement of $Ba_8Al_{14}Si_{31}$ showed that Al and Si share every framework site, with Al preferentially filling the 6c site. ^{27}Al MAS NMR provided further support for the Al site preference. The Seebeck coefficient, resistivity, and thermal conductivity data obtained at 300 K, taken together, yield a zT for $Ba_8Al_{14}Si_{31}$ of 0.010, which is low; however, it should be possible to improve these values by doping smaller atoms into the guest sites. Guest−host interactions should be diminished with the smaller guest atoms, thus causing the thermal conductivity to decrease, resulting in an improved zT.[3−10] Pressure has also been shown to enhance zT;[11−13] thus, adding a small element such as boron contributes chemical pressure to the structure. Additionally, we have also investigated the synthesis of $Ba_8Al_{14}Si_{31}$ and $EuBa_7Al_{13}Si_{33}$ by solid state synthesis, and high-temperature thermoelectric properties were measured which show promising results in which the absolute value of the Seebeck coefficient was found to give rise to reasonable zT values for $Ba_8Al_{14}Si_{31}$ with a maximum of 0.35 at 1150 K.[14] This promising zT value lends support to the importance of optimizing these phases further.

This paper presents efforts to affect the zT by incorporating boron into the framework. Recently, a borosilicide, $K_7B_7Si_{39}$, with a clathrate I structure has been reported.[15] In that case, there is enough boron in the structure to verify the composition with single-crystal X-ray diffraction, along with ^{11}B solid-state NMR spectroscopy. In the present example, only a small amount of boron is doped into the structure, and single-crystal X-ray diffraction could not distinguish the small amount of boron incorporated. Confirmation of boron-doping into $Ba_8Al_{14}Si_{31}$ is provided with elemental analysis and solid-state ^{11}B−^{27}Al spin echo double resonance (SEDOR)[20] NMR spectroscopy. In addition, the assignments of the resonances in the ^{27}Al NMR has been revised. The resistivity, Seebeck coefficient, and thermal conductivity as a function of temperature are also provided and compared with $Ba_8Al_{14}Si_{31}$.

Table 1. Atomic % of Elements from ICP Analysis[19] and Corresponding Compositions[a]

sample #	atom % of elements Ba	B	Al	Si	composition	lattice parameter a (Å)
CC1	44.5	0.0735	15.6	35.7	$Ba_{8.0}B_{0.1679}Al_{14.3}Si_{31.4}$[b]	10.6248(4)
CC2	44.5	0.0759	16.3	36.2	$Ba_{7.8}B_{0.1699}Al_{14.6}Si_{31.2}$[c]	10.6263(5)
CC3	44.0	0.0848	16.6	36.2	$Ba_{7.7}B_{0.1887}Al_{14.8}Si_{31.0}$[c]	10.6297(5)
CC4	44.4	0.140	15.5	34.6	$Ba_{8.0}B_{0.320}Al_{14.2}Si_{30.5}$[b]	10.6140(4)

[a] Lattice parameters (Å) obtained from Rietveld refinement of powder X-ray diffraction data for boron-doped $Ba_8Al_{14}Si_{31}$. [b] Ba = 8. [c] B + Al + Si = 46.

Experimental Section

Synthesis. Large single crystals (1−60 mg) of boron-doped $Ba_8Al_{14}Si_{31}$ were synthesized from the elements Ba (Johnson Matthey, 99.9%), B (Eagle Pitcher, 99.999999%), Si (AESAR, 99.999%), and Al (Matheson Colemen and Bell 99.6%) using the high-temperature metallic solution growth method.[16] All preparations were performed in a nitrogen-filled dry box with water levels less than 1 ppm. Elemental molar ratios (Ba/B/Al/Si) for the reactions are 2:5:70:30 (CC1), 2:10:70:30 (CC4), 2:15:70:30 (CC2), and 2:20:70:30 (CC3) scaled to 1 g of Al. Details of the heating procedures are the same as for $Ba_8Al_{14}Si_{31}$.[2] The designation of sample numbers follows the elemental analysis, indicating that CC4 contained the largest amount of boron. For NMR experiments, samples were prepared according to the same procedure with ^{11}B (Eagle Pitcher, 99.97%) that was first ground and cleaned in concentrated NaOH to remove any iron impurities. Residual flux was removed from all samples using a concentrated NaOH(aq) solution.

Single-Crystal X-Ray Diffraction. The single-crystal X-ray diffraction data for crystals from the reactions, CC1−CC4, were collected at ~90 K using a Bruker SMART 1000 CCD diffractometer employing graphite-monochromatized Mo Kα radiation (λ = 0.71069Å). Data were collected in the full sphere with 0.3° scans in ω and an exposure time of 10 s per frame. Lorentz and polarization effects were corrected for using the SAINT program, and absorption corrections were based on fitting a function to the empirical transmission surface as sampled by multiple equivalent reflections (program SADABS).[17] The structure solution was obtained by direct methods and refined by full-matrix least-squares refinement against F_0^2 using the SHELXTL 6.10 package.[17]

Powder X-ray Diffraction. X-ray powder diffraction data for boron-doped $Ba_8Al_{14}Si_{31}$ before hot pressing were collected with a Sintag PAD-V employing Cu Kα radiation. Data acquisition was performed with the WinAcq software. Sample analyses and Rietveld refinement of the data were performed using the REITICA software package.[18] The peak profile was chosen to be pseudo-Voigt (Howard asymmetry), and the background was fit to a fifth-order polynomial. Atomic positions as well as the overall temperature factors were held constant. The refined lattice parameters for the four samples are provided in Table 1. X-ray powder diffraction data after hot pressing are provided in the Supporting Information.

Thermal Analysis. A Netzsch thermal analysis STA 409 STA was used to evaluate the thermal properties between 25 and 1500 °C. After a baseline was established, several crystals ground into a

(3) Cohn, J. L.; Nolas, G. S.; Fessatidis, V.; Metcalf, T. H.; Slack, G. A. *Phys. Rev. Lett.* **1999**, *82*, 779.
(4) Sales, B. C.; Chakoumakos, B. C.; Jin, R.; Thompson, J. R.; Mandrus, D. *Phys. Rev. B: Condens. Matter Mater. Phys.* **2001**, *63*, 245113–1.
(5) Nolas, G. S.; Weakley, T. J. R.; Cohn, J. L.; Sharma, R. *Phys. Rev. B: Condens. Matter Mater. Phys.* **2000**, *61*, 3845.
(6) Blake, N. P.; Bryan, D.; Latturner, S.; Mollnitz, L.; Stucky, G. D.; Metiu, H. *J. Chem. Phys.* **2001**, *114*, 10063.
(7) Blake, N. P.; Latturner, S.; Bryan, J. D.; Stucky, G. D.; Metiu, H. *J. Chem. Phys.* **2001**, *115*, 8060.
(8) Blake, N. P.; Latturner, S.; Bryan, J. D.; Stucky, G. D.; Metiu, H. *J. Chem. Phys.* **2002**, *116*, 9545.
(9) Blake, N. P.; Mollnitz, L.; Kresse, G.; Metiu, H. *J. Chem. Phys.* **1999**, *111*, 3133.
(10) Blake, N. P.; Mollnitz, L.; Stucky, G. D.; Metiu, H. *Int. Conf. Thermoelectrics* **1999**, *18*, 489.
(11) Meng, J. F.; Shekar, N. V. C.; Chung, D. Y.; Kanatzidis, M.; Badding, J. V. *J. Appl. Phys.* **2003**, *94*, 4485.
(12) Meng, J. F.; Shekar, N. V. C.; Badding, J. V.; Chung, D. Y.; Kanatzidis, M. G. *J. Appl. Phys.* **2001**, *90*, 2836.
(13) Polvani, D. A.; Meng, J. F.; Shekar, N. V. C.; Sharp, J.; Badding, J. V. *Chem. Mater.* **2001**, *13*, 2068.
(14) Condron, C. L.; Kauzlarich, S. M.; Gascoin, F.; Snyder, G. J. *Chem. Mater.* **2006**, *18*, 4939.
(15) Jung, W.; Loerincz, J.; Ramlau, R.; Borrmann, H.; Prots, Y.; Haarmann, F.; Schnelle, W.; Burkhardt, U.; Baitinger, M.; Grin, Y. *Angew. Chem., Int. Ed.* **2007**, *46*, 6725.
(16) Canfield, P. C.; Fisk, Z. *Philos. Mag. B* **1992**, *65*, 1117.
(17) Sheldrick, G. M. *SADABS*; Bruker AXS: Madison, WI, 1999.
(18) Hunter, B. A. *IUCr Commission on Powder Diffraction Newsletter No. 20 (Summer)*; International Union of Crystallography: University Park, PA, 1998; 1.7.7. ed.
(19) *ICP Analysis*; Galbraith Laboratories: Knoxville, TN 37921-1700.
(20) Emshwiller, M.; Hahn, E. L.; Kaplan, D. *Phys. Rev.* **1960**, *118*, 414.

powder (40−60 mg) were placed in alumina crucibles and heated under argon at 10 K/min with an acquisition rate of 4 pts/K.

Inductively Coupled Plasma (ICP) and Scanning Electron microscopy (SEM). Inductively coupled plasma (ICP) analysis was used to identify the elemental ratios of the elements. Analysis was performed at Galbraith Laboratories Inc.[19] The results are summarized in Table 1. Energy dispersive X-ray (EDX) analysis results for Ba, Al, and Si were consistent with results from ICP analysis and are provided as Supporting Information.

NMR. NMR experiments were done in two different laboratories. A Bruker AVANCE spectrometer equipped with a fast digitizer was used with a Bruker high-speed MAS probe to collect ^{27}Al spectra (B_0 = 11.74 T). The sample was placed in a 2.5 mm Zirconia rotor. A one-pulse experiment was carried out with the sample spinning at 28.26 kHz. A 2 μs pulse was used at a resonance frequency of 130.316 MHz. The 90° pulse was found to be 4 μs, and a total of 5816 scans were collected with a 0.5 μs dwell time and a 0.2 s relaxation delay. The Bruker XWINNMR3.5 software was used to record and process the data.

Bruker AVANCE and TecMag APOLLO spectrometers were used with magnetic fields of B_0 = 11.74 T and B_0 = 7.04 T, respectively. ^{11}B and ^{29}Si experiments were performed exclusively at the higher magnetic field with corresponding resonance frequencies of about 160.464 and 99.364 MHz. The ^{27}Al resonance frequencies are 130.321 and 78.193 MHz in the high and the low magnetic field, respectively.

Samples were enclosed into 2.5 mm ZrO_2 rotors for MAS experiments and into a quartz container of 5 mm diameter. To reduce possible eddy currents during MAS experiments and the skin effect of the electronic conducting material during wide-line experiments, the compounds were diluted with GeO_2.

Wide-line experiments, to analyze the line shape of the signals, were done in a probe optimized for the detection of a large frequency range equipped with a Manganin coil to reduce the quality factor of the probe built by NMR service (Erfurt, Germany). ^{11}B−^{27}Al SEDOR[20] experiments, to measure internuclear dipole−dipole couplings, were made in a double-resonance probe suited for nonsimultaneous excitation of close frequencies as for ^{11}B and ^{27}Al. The probe was built by NMR service (Erfurt, Germany) using a design introduced by Jürgen Haase.[21] MAS and multiple-quantum MAS (MQMAS) experiments, to enhance signal resolution and intensity, were done in a 2.5 mm standard triple-resonance probe (Bruker, Germany).

Wide-line experiments on ^{11}B and ^{27}Al were performed applying an echo sequence with pulses of an equal duration of 3.0 and 1.5 μs, respectively. An interpulse delay of τ = 30 μs was used for both nuclei. ^{27}Al MAS measurements were carried out with rotation frequencies ν_{rot} = 28.5 kHz applying a single-pulse sequence with a pulse duration of 2 μs and ν_{rot} = 35 kHz with a rotor frequency synchronized echo sequence with pulses of 1.5 μs duration. The ^{29}Si MAS experiments were done with 35 kHz rotation frequency using a pulse Hahn-Echo pulse sequence with pulses of 1.0 and 2.0 μs duration. ^{11}B was observed while ^{27}Al nuclei were used for probing the heteronuclear dipole−dipole couplings in the SEDOR experiments. The pulses' duration for observation was 3.0 μs as a π/2 pulse, and that for manipulation was 4.9 μs as a π pulse. A three-pulse sequence was employed in ^{27}Al MQMAS with pulse durations of 3.4 μs for excitation, 1.4 μs for conversion, and 12.5 μs for the selective detection pulse. A sheared transformation was applied to analyze the signals. All NMR experiments but the MQMAS measurements were done by 8-fold phase cycling of the pulse sequences. Twelve-fold phase cycling was applied in the MQMAS experiments.

While for ^{27}Al a cycle delay of 0.5 s was sufficient, for ^{11}B, a 3 s and, for ^{29}Si, a 2 s cycle delay had to be used to ensure full relaxation of the magnetization. About 65 k scans were used for the ^{27}Al wide line, and 20 k scans were used for the MQMAS experiments. Due to the low natural abundance of ^{29}Si, about 128 k scans were applied, and due to the low B content of the samples, about 60 k scans were applied. The Bruker TopSpin 2.0 software was used to record and process the data.

Thermoelectric Property Sample Preparation. In order to obtain dense samples, finely ground polycrystalline powder was hot-pressed in high-density graphite dies (POCO). A cylinder ~6.5-mm-long and 12 mm in diameter was obtained. The experimental density (calculated from measured dimensions and weight) was found to be ~95% of the theoretical density. Hot-pressing was conducted at ~20 000 psi and 1223 K for 1.5 h under argon.

For electrical and thermal transport properties, discs (typically a 1-mm-thick and 12-mm-diameter slice) were cut from the cylinder using a diamond saw. Seebeck coefficient measurements were performed on the remaining cylinder. All physical properties were measured between room temperature and 1273 K.

Thermoelectric Properties Measurements. The electrical resistivity (ρ) was measured using the van der Pauw technique with a current of 100 mA and a special high-temperature apparatus.[22] The Seebeck coefficient (α) was measured using a high-temperature light pulse technique using W/Nb thermocouples.[23]

The thermal diffusivity was measured for several samples using a flash diffusivity technique.[24] The heat capacity was estimated using the model of Dulong and Petit, $C_p = 3\ k_B$, for each atom. The thermal conductivity (λ) was calculated from the calculated heat capacity, experimental density, and experimental thermal diffusivity values. Data were measured to 1223 K and extrapolated to 1300 K.

Results and Discussion

Figure 1 provides a view of the crystal structure of type I clathrate. Inorganic clathrates containing groups 13 and 14 have been prepared by direct reaction of the elements, flux growth, and Czochralski growth.[2,14,25−28] It has been suggested for $Ba_8Al_{16}Ge_{30}$ that the flux-grown crystals have the lowest aluminum content.[27] In the case of boron-doped Ba−Al−Si clathrate phase obtained from an Al flux, all of the samples have compositions closer to $Ba_8Al_{14}Si_{31}$. This formula is consistent with what we have obtained via flux for the undoped system. Although a significant amount of boron was added to the flux, only a small amount appears to be incorporated into the lattice. Table 1 provides the compositions as determined from ICP analysis[19] for the four samples investigated. The formulas were normalized either

(21) Haase, J.; Curro, N. J.; Slichter, C. P. *J. Magn. Reson.* **1998**, *135*, 273.
(22) McCormack, J. A.; Fleurial, J. P. *Mater. Res. Soc. Symp. Proc.* **1991**, *234*, 135.
(23) Wood, C.; Zoltan, D.; Stapfer, G. *Rev. Sci. Instrum.* **1985**, *56*, 719.
(24) Vandersande, J. W.; Wood, C.; Zoltan, A.; Whittenberger, D. *Thermal Conductivity* **1988**, *19*, 445.
(25) Mudryk, Y.; Rogl, P.; Paul, C.; Berger, S.; Bauer, E.; Hilscher, G.; Godart, C.; Noel, H.; Saccone, A.; Ferro, R. *Physica B* **2003**, *328*, 44.
(26) Mudryk, Y.; Rogl, P.; Paul, C.; Berger, S.; Bauer, E.; Hilscher, G.; Godart, C.; Noel, H. *J. Phys. (Paris)* **2002**, *14*, 7991.
(27) Christensen, M.; Iversen, B. B. *Chem. Mater.* **2007**, *19*, 4896.
(28) Condron, C. L.; Kauzlarich, S. M. *Inorg. Chem.* **2007**, *46*, 2556.

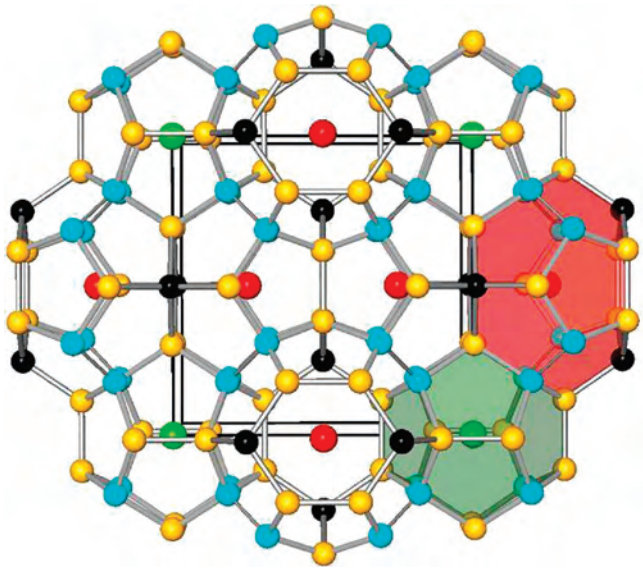

Figure 1. Illustration of the type-I clathrate unit cell. The elements and atomic positions are indicated by color. Ba: 2a = green and 6d = red. Si/Al/B: 6c = black, 16i = cyan, and 24k = orange.

to full occupancy of Ba or full occupancy of the framework sites when normalizing to eight Ba, resulting in a greater than 46-atom framework composition. On the basis of the experimental elemental composition, all samples can be considered as having full guest occupancies, and nearly full framework occupancies. Overall, the amount of boron is quite small, with two of the samples being approximately the same (CC1 and CC2), with the approximate composition $Ba_8B_{0.17}Al_{14}Si_{31}$, one with a slightly higher B content, (CC3) $Ba_8B_{0.19}Al_{15}Si_{31}$, and the highest B content (CC4) having the approximate composition $Ba_8B_{0.32}Al_{14}Si_{30}$. The fact that an intermediate loading of boron provided the largest amount of incorporated boron suggests that details such as temperature, heating rates, and flux homogeneity are important for the composition of crystals in the final product. Figure 2a−d displays the back-scattered electron image (BSEI) of the polished pellets for CC1−CC4, respectively. The compositions are homogeneous for all of the samples; the observed dark spots are due to residual SiC used to polish the samples' surface as well as holes or cracks in the pellet.

Single-crystal X-ray diffraction indicated that the crystals were all type-I clathrate structures; however, the boron content could not be determined due to the difficulties of distinguishing between Al and Si, as well as finding small amounts of the light element B in the presence of heavier atoms. Since the amount of Al and Si could not be determined without ambiguity from combined single-crystal X-ray and neutron diffraction,[2] it was not surprising that we could not locate the boron in the structure. Powder X-ray diffraction experiments were used to determine phase purity as well as room temperature lattice parameters (Table 1). Several clean crystals of each sample were selected and ground into sufficient particle size for powder X-ray diffraction analysis. Figure 3 shows the Rietveld profile fits for CC1 and CC4, respectively. Data for CC2 and CC3 are similar, and the fit to the data is provided in the Supporting Information. All samples crystallize with the type-I clathrate structure, and although the patterns are very similar, there are subtle differences in peak intensities (peaks marked with a ∗), suggesting that boron is being incorporated into the crystal structure. CC1−CC3 have similar amounts of boron and similar lattice parameters. CC4 has the largest amount of B and gives the smallest lattice parameter, as expected. Compared with the parent phase, $Ba_8Al_{14}Si_{31}$ (a = 10.6373 (10) Å), all four samples have slightly reduced lattice parameters. Powder X-ray diffraction of the samples after hot pressing does not change, confirming that the samples do not degrade during the hot pressing process (see the Supporting Information).

Differential scanning calorimetry (DSC) scans for CC1 and CC4 are shown in Figure 4a and b, respectively. The DSC curves suggest that these phases melt above 1400 K, with the highest melting point of 1424 K for CC4, corresponding to the phase with the highest B content. There is no evidence for additional phase changes, with the exception of small amounts of Al/Si eutectic that was not completely removed during the cleaning process (concentrated NaOH (aq)), indicating that this clathrate phase melts congruently. The Al/Si eutectic was identified by the very small melting and crystallization observed in the data at approximately 845 K.[29] X-ray powder diffraction of the sample after melting shows that the sample remains as a clathrate-I structure. There is no evidence of weight loss or weight gain in the thermogravimetric analysis scans.

Figure 5a−d shows the ^{27}Al MAS NMR spectrum for CC1, CC2, CC3, and CC4, respectively. The line shape of the signal in the range between 150 and 650 ppm indicates that the signal is composed by several contributions. The signal at approximately 1600 ppm is symmetric and shows rotational side bands being not observed for the other signal contribution at a low shift. The signal is exactly at the position of Al metal.[30] It can be most probably assigned to Al remaining as Al/Si eutectic in the sample from the flux, although we have previously assigned it to the Al in the most symmetric, 6*c* crystallographic site.[2] The presence of Al/Si eutectic is also indicated by the thermal investigations showing an endothermic peak at about 850 K,[29] noted above. The main signal contributions are above the range expected for the chemical shielding of ^{27}Al, being about ±200 ppm.[31] Therefore, the signals show a Knight shift, indicating that the Al atoms in the framework are interacting with the conduction electrons.

The signal in the frequency range from 150 to 650 ppm was investigated in more detail for sample CC1 (Figure 6). It is assigned to the main transition signal of a quadrupole nucleus (I > 1/2) exposed to an electric field gradient. No characteristic features of the satellite transitions were observed, despite a broad background. This indicates a large amount of disorder in the crystal structure. The line shape of the main transition signals is not influenced by a change

(29) Murray, J. L.; McAlister, J. *Binary Alloy Phase Diagrams*, 2nd ed.; AMS International: Materials Park, OH, 1990; Vol. *1*.
(30) Winter, J. *Magnetic Resonance in Metals*; Oxford University Press: New York, 1971.
(31) Mason, J. *Multinuclear NMR*; Kluwer Academic/Plenum Publishers: Norwell, MA, 1987.

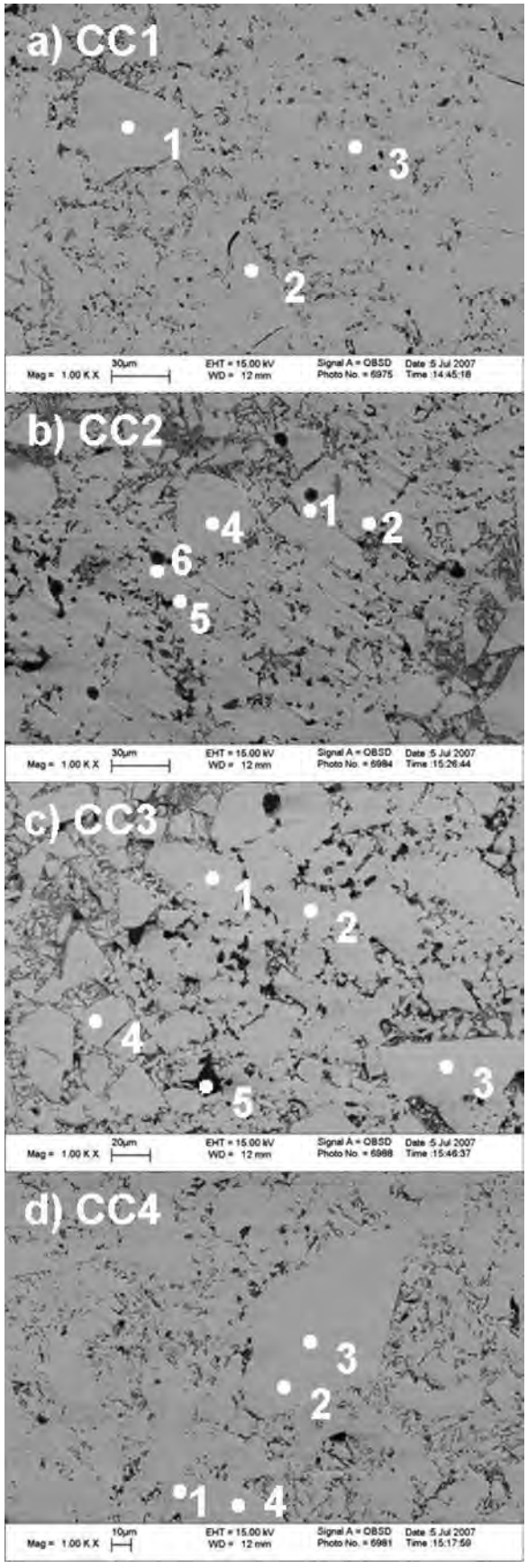

Figure 2. Back-scattered electron images (BSEI) for the polished hot-pressed pellets. Energy dispersive X-ray (EDX) analysis was obtained for each of the points marked with numbers and indicated that the samples were homogeneous. Scale bar is 30 μm for all of the BSEI. EDX results are provided as Supporting Information.

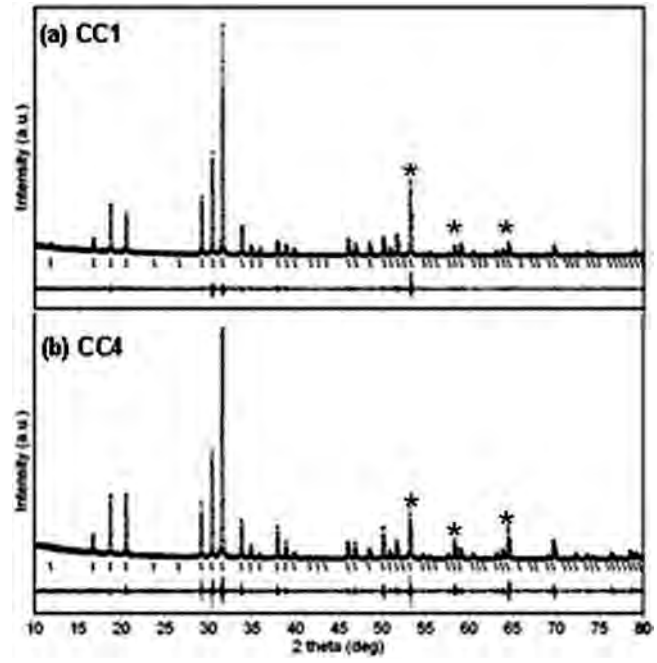

Figure 3. Rietveld profile fit for X-ray powder diffraction patterns of boron-doped $Ba_8Al_{14}Si_{31}$, (a) CC1 and (b) CC4. Experimental data points are shown as black circles, and the theoretical fit is shown as a gray solid curve. A $*$ indicate peaks that change in amplitude upon boron doping. The data were refined for the space group $Pm\bar{3}n$ (black ticks), and the difference between the observed and theoretical patterns is shown below the black ticks. CC1: $R_p = 10.4\%$, $R_{wp} = 15.1\%$, $R_{Bragg} = 1.5\%$, $\chi^2 = 1.45$. CC4: $R_p = 14.5\%$, $R_{wp} = 21.2\%$, $R_{Bragg} = 1.1\%$, $\chi^2 = 2.631$.

of the applied magnetic field (Figure 6a). This indicates that the signal width is due to a distribution of shifts being proportional to the magnetic field. Furthermore, a significant second-order contribution of the quadrupole coupling of nuclei exposed to a large electric field gradient can be excluded. The width of the signal should become larger at the lower field if second-order quadrupole coupling is the source of signal broadening. High-speed MAS with a rotation frequency of 35 kHz removing almost all homonuclear and heteronuclear couplings shows a small shrinkage of the signal, being also in agreement with a signal composed by a shift distribution. Two contributions are clearly visible, and a third one is indicated as a shoulder at high frequencies. MQMAS experiments, refocusing only the quadrupolar coupling, result in a broad distribution of signals. These are aligned along the diagonal determined by the isotropic shift (Figure 6b). Three of the individual signal contributions, extracted as traces parallel to the F2 direction, are also depicted in Figure 6a. From this, it can be concluded that only small quadrupolar coupling influences the width of the signals. The estimated quadrupole coupling constant $P_Q = 0.40(5)$ MHz is relatively small. The center of gravity method used for data analysis does not allow a separation of the asymmetry and the anisotropy parameter of the quadrupole coupling constant. Three regions of slightly different quadrupole couplings were observed in the signal. These correspond to the regions seen by the line-shape analysis of the MAS signal. In order to be more sensitive to the second-order quadrupole coupling, determining the width of the individual signal contributions, MQMAS experiments with

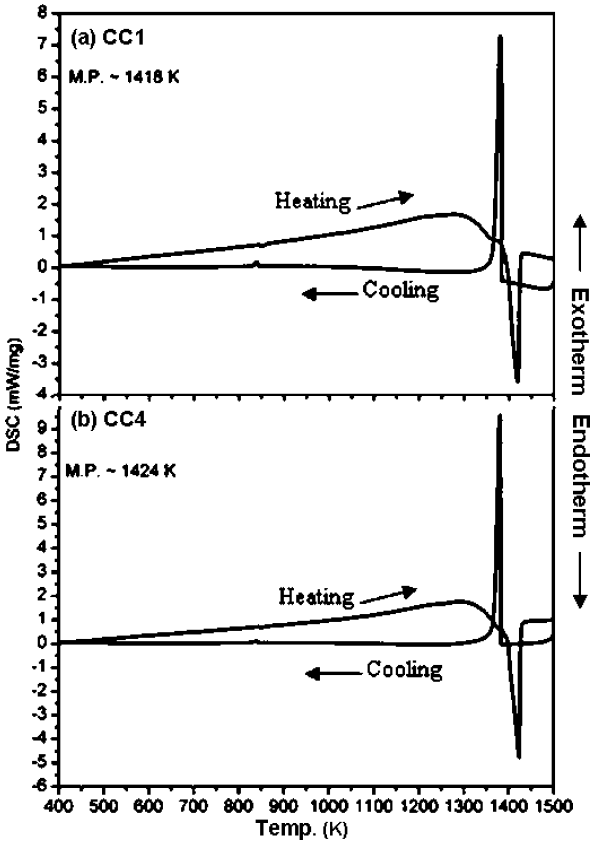

Figure 4. Differential scanning calorimetry (DSC) traces as a function of temperature for boron-doped $Ba_8Al_{14}Si_{31}$ (a) CC1 and (b) CC4. Data were obtained by heating/cooling at a rate of 10 K/min under flowing argon. Arrows indicate heating and cooling data.

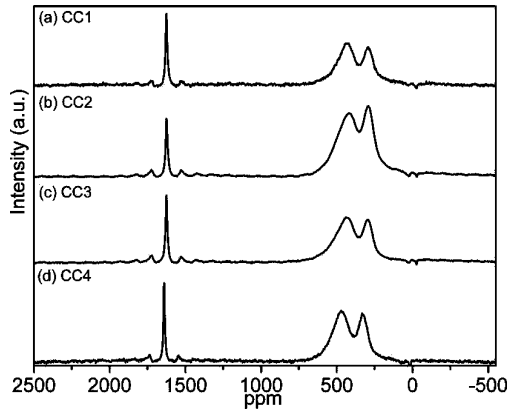

Figure 5. ^{27}Al MAS NMR spectra of boron-doped $Ba_8Al_{14}Si_{31}$. a, b, c, and d display CC1, CC2, CC3, and CC4, respectively.

rotation frequencies of about 35 kHz using a magnetic field of about 2 T have to be done.

Considering all of the ^{27}Al NMR experiments, we can propose a model describing the signal in the region from 150 to 650 ppm as a superposition of signals of chemically very similar nuclei. Three regions can be identified corresponding to the number of nonequivalent crystallographic sites in the clathrate framework. The distributions of frequencies indicate a large amount of slightly different local environments. Their small differences are due to a nonregular connectivity of the atoms in the framework. Furthermore, a disorder introduced by small shifts of the cations from the

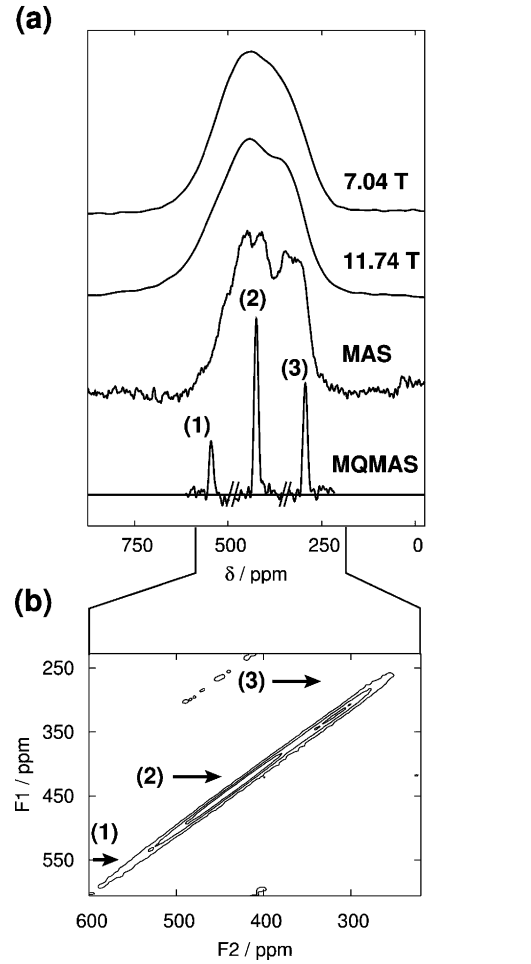

Figure 6. ^{27}Al NMR signals of sample CC1. (a) From the top: wide-line experiments' measured magnetic fields $B_0 = 7.04$ T and $B_0 = 11.74$ T; MAS spectrum for $\nu_{rot} = 35$ kHz rotation frequency and $B_0 = 11.74$ T; slices extracted from the MQMAS experiment. (b) MQMAS spectrum using $\nu_{rot} = 35$ kHz. The F1 frequencies corresponding to the extracted slices in a are marked by arrows.

center of the cages has to be considered. Similar distributions of shifts have been observed in the tin clathrates $M_8Sn_{44}\square_2$ with M = K, Rb, and Cs and in the inverse clathrates $Sn_{17}Zn_7P_{22}X_8$ with X = I and Br.[32] An assignment of the signal regions to the sites of the clathrate structure cannot be given, due to the complexity of the various interactions causing the signal shift, for example, Knight shift and chemical shielding.

The ^{11}B signals of samples CC1, CC2, CC3, and CC4 are depicted in Figure 7. The signals are shifted by about 40 ppm with respect to the reference compound. A relatively narrow main transition signal is located on top of a background, covering a large frequency range. This background is most probably due to the satellite transitions being smeared by distributions of quadrupole couplings as for the ^{27}Al signal. Focusing on the main transition, two contributions of varying intensity ratios can be seen. This indicates that boron is located on at least two sites or that, due to the local bonding situation, two chemically nonequivalent posi-

(32) Kovnir, K. A.; Shatruk, M. M.; Reshetova, L. N.; Presniakov, I. A.; Dikarev, E. V.; Baitinger, M.; Haarmann, F.; Schnelle, W.; Baenitz, M.; Grin, Y.; Shevelkov, A. V. *Solid State Sci.* **2005**, *7*, 957.

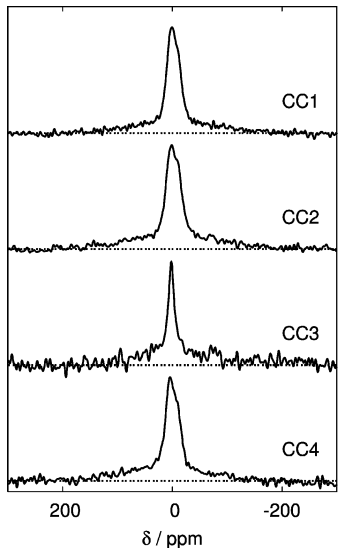

Figure 7. ^{11}B wide-line NMR signals for the various samples of boron-doped $Ba_8Al_{14}Si_{31}$ (CC1, CC2, CC3, and CC4).

tions exist as in $K_7B_7Si_{39}$.[15]

SEDOR experiments are suited to measure internuclear dipole−dipole couplings being inversely proportional to the third power of the distance of the interacting nuclei. These have to be in the order of a few ångstroms to result in a measurable influence. The signal amplitude of an echo experiment on the ^{11}B nuclei (S_0) is compared with an echo experiment (S) probing the heteronuclear dipolar coupling by excitation of the ^{27}Al nuclei. Figure 8 shows the SEDOR decay (S/S_0) for sample CC1, being proof that boron is incorporated into the clathrate framework and not part of a secondary phase. Due to the limited signal-to-noise ratio, a different decay of the signal contributions could not be observed.

The ^{29}Si NMR signal of sample CC1 is depicted in Figure 9. Three signal contributions being in agreement with the number of sites in the clathrate framework are visible. The signals are shifted by 204, 123, and −13 ppm with respect to TMS as a reference compound. Compared to the signals of ^{29}Si in Na_8Si_{46} being unambiguously influenced by a Knight shift,[33] this is a small amount (842, 653, and 617 ppm). The width of the individual signal contributions is relatively large, indicating a large amount of disorder in the compound.

The temperature dependencies of the electrical resistivity and Seebeck coefficient are shown in Figure 10a and b, respectively. All three possess *n*-type conductivity, and the electrical resistivity increases with increasing temperature, characteristic of metallic behavior, up to ∼1065 K, where the resistivity begins to decrease. The samples show increased resistivity but similar Seebeck coefficients compared with the undoped $Ba_8Al_{14}Si_{31}$ prepared via direct reaction of the elements. CC1 and CC4 have nearly the same resistivity through the entire temperature range, while CC2 is close to CC1 and CC4 up to ∼876 K, where the magnitude

(33) Ramachandran, G. K.; McMillan, P. F.; Diefenbacher, J.; Gryko, J.; Dong, J. J.; Sankey, O. F. *Phys. Rev. B: Condens. Matter Mater. Phys.* **1999**, *60*, 12294.

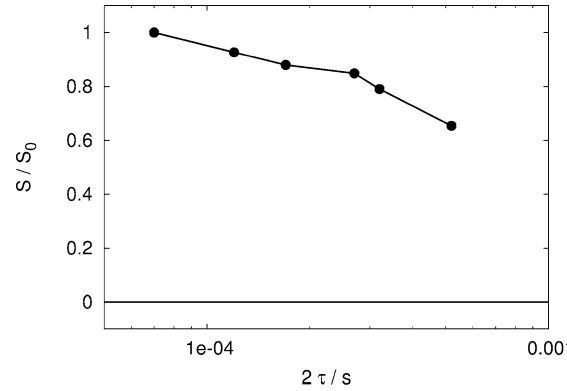

Figure 8. Normalized SEDOR decay (S/S_0) of sample CC1. The heteronuclear coupling of the ^{11}B to the ^{27}Al nuclei was probed in the experiments, while ^{11}B was the observed nucleus.

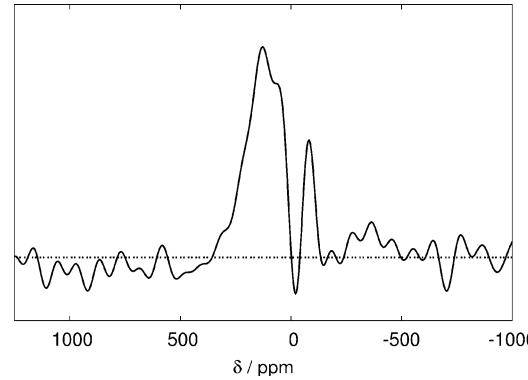

Figure 9. ^{29}Si NMR signals of sample CC1.

of the resistivity becomes larger. The magnitude of the resistivity for CC3 is higher through the whole temperature range. The absolute value of the Seebeck coefficient, $|S|$, gradually increases with increasing temperatures, with CC2 having the highest absolute value at ∼95 μV/K. The increase in resistivity is primarily due to a temperature-independent term, while the slopes of the resistivity with temperature curves are essentially the same and similar to that of the undoped $Ba_8Al_{14}Si_{31}$.[14] This suggests that temperature-independent grain boundary resistance causes the increased resistance. The fact that the Seebeck coefficients are similar suggests that the carrier concentration and effective mass does not change with these or the undoped sample.

There are two components to the thermal conductivity; the electronic component (κ_e) depends on the electrical conductivity and can be estimated using the Wiedemann−Franz law, $\kappa_e = L_0T(1/\rho)$, where L_0 is the Lorenz number ($L_0 = 2.44 \times 10^{-8}$ W Ω K^{-2}), ρ is the electrical conductivity, and T is the absolute temperature in degrees Kelvin. The second component is the lattice component (κ_L) and depends on structural details and bonding. Figure 11 shows the lattice, κ_L, (closed symbols) found by subtracting κ_e from κ, and the electronic, κ_e (opened symbols), components to the thermal conductivity for CC2 (triangles), having the highest zT value, and CC3 (circles), having the lowest zT value. Note that these were calculated by extracting values from polynomial fits of the raw data so that the entire temperature range would be represented. For both phases, κ_e and κ_L are closer in value at these temperatures than their parent phase,[14]

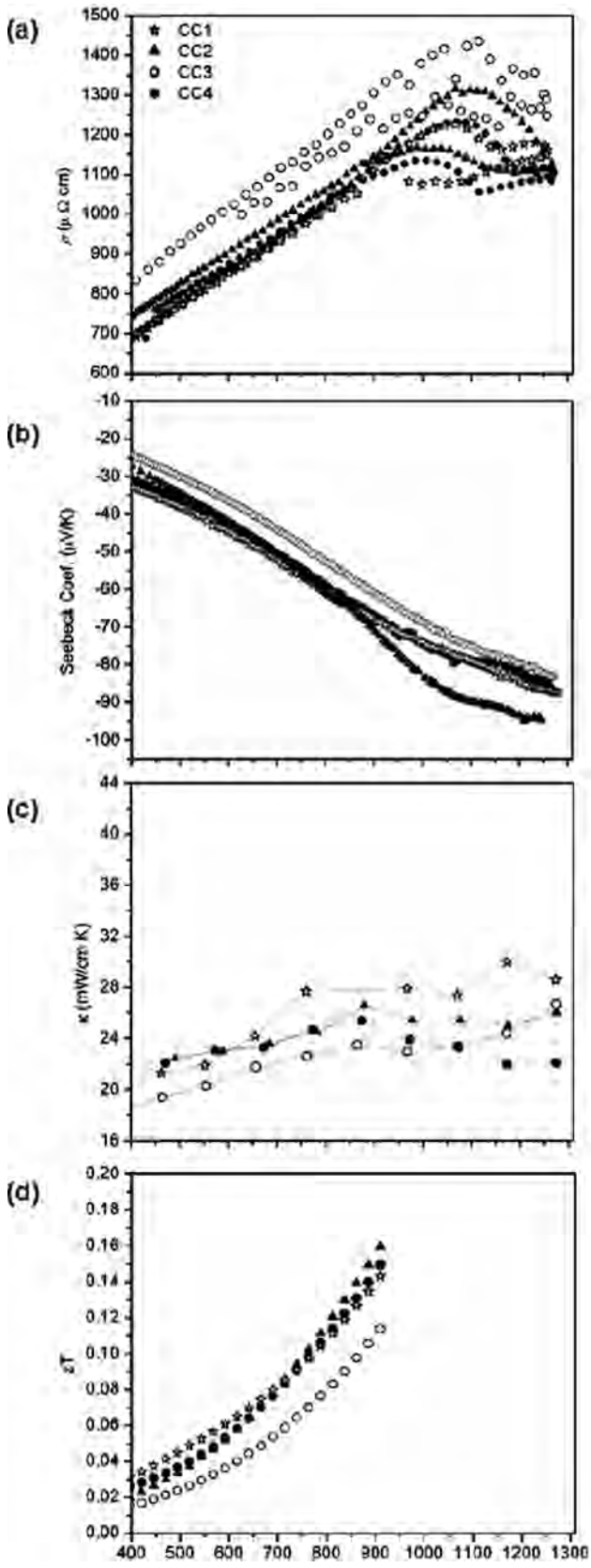

Figure 10. Temperature dependence of the (a) resistivity, (b) Seebeck coefficient, (c) thermal conductivity, and (d) dimensionless figure of merit for CC1 (stars), CC2 (triangles), CC3 (open circles), and CC4 (closed circles).

and the electronic component dominates.

Figure 10c shows that the total thermal conductivities

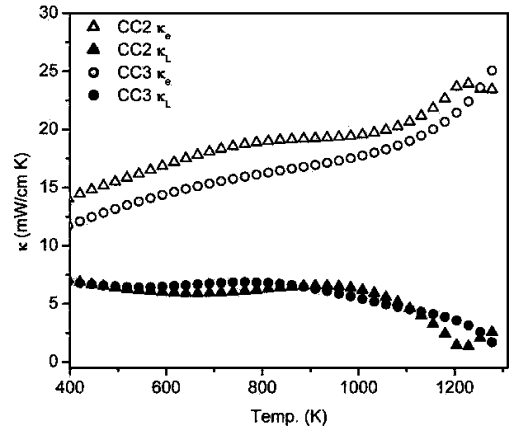

Figure 11. Temperature dependence of the lattice (closed symbols) and electronic (open symbols) components of the thermal conductivity for CC2 and CC3.

(lines are a guide for the eye) for CC1−CC4 have similar (although scattered) thermal conductivity values that are slightly lower than that of their parent phase $Ba_4Al_{14}Si_{31}$.[14] The thermal conductivity values are slightly higher than what is observed for $Ba_8Ga_{16}Ge_{30}$ single crystals over the same temperature range.[34,35] The larger thermal conductivity values, as compared to $Ba_8Ga_{16}Ge_{30}$, are attributed to the smaller, less massive framework atoms forming smaller, lighter polyhedra. Above ~1072 K, CC1 and CC4 have the highest and lowest κ, respectively, while CC2 and CC3 have nearly the same values. zT for CC1−CC4 (extracted from polynomial fits of the raw data) is shown in Figure 10d. At ~900 K, CC2 has the highest zT value at ~0.17, while CC3 has the lowest at ~0.11. It would be meaningful if a trend in the properties was apparent with increasing boron content, such that the magnitude of the resistivity increased (likewise $|S|$ and zT) with the addition of boron. Such a trend is not apparent, making data evaluation difficult. However, the amount of boron incorporated is small, and therefore, it is not expected to have a significant effect on thermal conductivity. Qualitatively, CC2 and CC4 have zT's that increase more rapidly than CC1 and CC3. CC2 has the highest $|S|$ and is in the middle for ρ and κ, implying that the higher $|S|$ is driving the high zT. For CC4, the low ρ and κ are the reason for the enhanced zT. Thus, CC1 and CC3 suffer from having average ρ, $|S|$, and κ. Additionally, it is worth noting that the thermoelectric properties are possibly being hindered by the powdering and hot pressing parameters as the BSEIs of the hot-pressed pellets exhibit holes and cracks that likely increase κ, and reduce $|S|$. We thus propose that the thermoelectric properties are lower than expected because grain boundaries are affecting the transport properties. It would be interesting to see if the thermoelectric properties could be enhanced under optimal powdering and pressing conditions.

(34) Saramat, A.; Svensson, G.; Palmqvist, A. E. C.; Stiewe, C.; Mueller, E.; Platzek, D.; Williams, S. G. K.; Rowe, D. M.; Bryan, J. D.; Stucky, G. D. *J. Appl. Phys.* **2006**, *99*.

(35) Toberer, E. S.; Christensen, M.; Iversen, B. B.; Snyder, G. J. *Phys. Rev. B: Condens. Matter Mater. Phys.* **2008**, 77.

Summary

Single crystals of boron-doped $Ba_8Al_{14}Si_{31}$ were synthesized using the molten flux technique. Powder X-ray diffraction confirmed that all of the phases crystallize with the clathrate type-I structure. Compositions were determined from ICP analysis, and the phase purity was confirmed with powder X-ray diffraction and SEM. Multinuclear NMR indicates that boron is doped into the framework. High-temperature thermoelectric measurements on hot-pressed pellets show increased resistivity with little change to the Seebeck coefficient or thermal conductivity. These results are attributed to grain boundaries in the hot-pressed pellets. Optimization of the pellet pressing parameters may provide improved properties, giving rise to higher zT's than reported herein.

Acknowledgment. The authors gratefully acknowledge Dr. Alexandra Navrotsky (Department of Chemistry and Thermochemistry Facility and NEAT ORU, University of California Davis) for use of the Scintag powder diffractometer. This work was supported by the National Science Foundation (Grant DMR-0600742). C.L.C. acknowledges a Tyco Electronics Foundation Fellowship in functional materials. Portions of this work were carried out at the Jet Propulsion Laboratory, California Institute of Technology, under a contract with NASA. P.J. acknowledges financial support by the Alexander von Humboldt foundation.

Supporting Information Available: Rietveld refinement of powder X-ray diffraction, a table of EDX values from SEM BSEI of hot pressed pellets, powder X-ray diffraction after hot pressing, and TG/DSC for all samples not already reported in the manuscript/ This material is available free of charge via the Internet at http://pubs.acs.org.

IC800772M